JOURNAL OF AIRCRAFT
Vol. 46, No. 4, July–August 2009

Passive Control of the Flow Around the Stratospheric Observatory for Infrared Astronomy

Sven Schmid,* Thorsten Lutz,† and Ewald Krämer‡
Universität Stuttgart, 70569 Stuttgart, Germany
and
Timo Kühn§
German Aerospace Center, 38108 Braunschweig, Germany

DOI: 10.2514/1.40777

The unsteady flowfield around the Stratospheric Observatory for Infrared Astronomy, a reflecting telescope carried inside an open port of a Boeing 747SP, has been simulated by means of detached eddy simulations and unsteady Reynolds-averaged Navier–Stokes simulations. Vortex generators have been placed upstream of the cavity to control the shear layer spanning the opening. The influence of baffles and displacement bodies placed inside the telescope port on the frequencies of acoustic resonant modes was investigated by acoustic simulations, based on the solution of the homogenous Helmholtz equation. The objective of this study is to improve the telescope's performance by mitigating the amplitudes and changing the characteristic frequencies of the pressure fluctuations inside the cavity. The present simulations show that the investigated measures have a high potential to increase the telescope's pointing stability.

Nomenclature

c	=	speed of sound, m/s
D	=	cavity depth, m
f	=	frequency, Hz
i	=	imaginary part
K	=	nondimensional convection speed
k	=	dimensionless frequency
L	=	cavity length, m
l_{ref}	=	reference length, m
M	=	Mach number
m, n	=	mode number
p	=	pressure, Pa
t	=	time, s
U	=	velocity, m/s
W	=	cavity width, m
y^+	=	nondimensional wall distance
γ	=	phase delay
δ_2	=	momentum thickness, mm
ϕ	=	velocity potential
ω	=	angular frequency, Hz

I. Introduction

NASA and the DLR, German Aerospace Center are working together to create and operate the Stratospheric Observatory for Infrared Astronomy (SOFIA), a reflecting telescope located inside a Boeing 747SP aircraft (see Fig. 1). During observation in the stratosphere, a door in the fuselage will be opened to expose the infrared telescope to the atmosphere. In general, the flow over cavities such as the SOFIA telescope port is characterized by unsteady flow phenomena associated with prominent pressure fluctuations caused by amplified acoustic resonances. In the present case, this phenomenon causes unwanted vibrations of the telescope structure and reduces its pointing stability. Flow control in the case of SOFIA is performed by a slanted cavity rear wall that stabilizes the shear layer's impingement point and prevents it from oscillating violently. Several wind-tunnel studies on 3 and 7% models have proven the concept to be effective and robust to deviations from the nominal flow state. The objective of the present numerical investigations is to estimate the remaining potential to further increase the performance of the system by changing the shear layer's stability characteristics and by shifting the acoustic resonant frequencies away from resonance modes of the telescope structure.

Presented as Paper 6717 at the 26th AIAA Applied Aerodynamics Conference, Honolulu, Hawaii, 18–21 August 2008; received 3 September 2008; revision received 17 February 2009; accepted for publication 8 March 2009.

*Research Engineer, German Stratospheric Observatory for Infrared Astronomy Institute. Member AIAA.
†Senior Researcher, Institute of Aerodynamics and Gas Dynamics, Pfaffenwaldring 21. Member AIAA.
‡Professor, Head of the Institute, Institute of Aerodynamics and Gas Dynamics, Pfaffenwaldring 21. Member AIAA.
§Research Engineer, Institute of Aerodynamics and Flow Technology, Lilienthalplatz 7.

II. Characteristics of Unsteady Cavity Flow and Acoustics

The flow over cavities in general is characterized by self-sustained pressure fluctuations. The shear layer spanning the opening of the cavity amplifies flow disturbances convecting downstream, which are scattered into acoustic waves at the downstream edge. These waves propagate upstream inside and outside the cavity and excite further disturbances in the shear layer to create a feedback loop. Frequencies with a phase lag of a multiple of 2π are being amplified, yielding a selection of discrete modes. Rossiter [1] found that the frequencies can be represented by the semi-empirical equation

$$f = \frac{U}{L}\frac{(m-\gamma)}{\frac{1}{k}+M}, \qquad m = 1, 2, 3, \ldots \tag{1}$$

where γ and k are empirical constants. γ represents the phase delay of shear layer disturbances that are scattered at the downstream edge; their convection speed is k times the freestream speed. The existence and the magnitude of these Rossiter modes depend mainly on the stability characteristics of the shear layer that evolves from the boundary layer in front of the cavity [2], basically the momentum thickness δ_2. Small values in general lead to higher shear layer disturbance amplification and, hence, to higher fluctuation levels inside the cavity. If the Rossiter modes' frequencies coincide with the acoustic cavity resonant frequencies, standing waves can be excited,

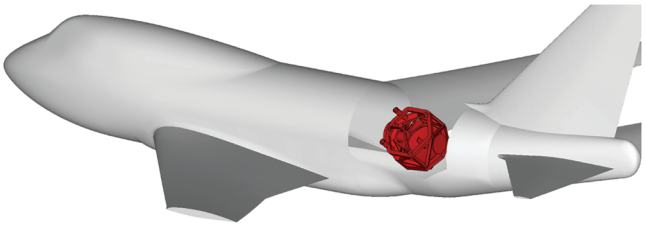

Fig. 1 SOFIA, the reflecting infrared telescope carried by a Boeing 747SP.

leading to a "lock in" at the characteristic resonant frequencies [3]. This effect enhances the feedback of disturbances and thereby increases the pressure amplitudes. For a rectangular cavity, the acoustic resonant frequencies can be predicted analytically by

$$f = \frac{c}{2} \cdot \sqrt{\left(\frac{n_x}{L}\right)^2 + \left(\frac{n_y}{2D}\right)^2 + \left(\frac{n_z}{W}\right)^2} \tag{2}$$

where $n_x = n_y = 1, 2, 3, \ldots$ and $n_z = 0, 1, 3, 5, \ldots$ represent the mode numbers [4]. The amount of acoustic energy radiated to the far field depends on the ratio between the opening surface and the cavity volume. The deeper the cavity and the smaller the opening relative to its volume, the more acoustic energy is conserved and the more the cavity is dominated by acoustic resonances.

Figure 2 shows the Strouhal number of the Rossiter modes and the acoustic modes of a rectangular two-dimensional cavity, according to Eqs. (1) and (2). At different Mach numbers, the frequencies of the excitation and the acoustic response coincide (marked as black dots in the diagram). In these regions, the excitation of acoustic waves is likely and the sound-pressure levels inside the cavity are increased. As a cavity has a multitude of resonance modes at different frequencies, there is a certain likelihood that at least one of the Rossiter modes is close to any of the resonance modes and that acoustic resonance modes are excited. Regarding the SOFIA configuration, it is likely that there is a further coincidence between the acoustic and structural modes of the telescope that may significantly affect observing conditions.

III. Modelling Approach

A. Computational Fluid Dynamics Simulation

The present numerical flow simulations were carried out with the flow solver TAU that was developed by the DLR, German Aerospace Center [5]. The code is based on a dual-grid cell-vertex formulation and solves the unsteady, compressible, three-dimensional Navier–Stokes equations on unstructured grids. Several turbulence- and subgrid-scale models are provided by TAU for Reynolds-averaged Navier–Stokes (RANS) simulations, large eddy simulations (LES), and detached eddy simulations (DES). In the present RANS computations, flow turbulence is modeled by the Menter–shear stress transport turbulence model, which has shown the best performance compared with other two-equation models in previous cavity flow studies performed by the present authors [6,7]. For the DES simulations, the Spalart–Almaras subgrid-scale model was used. The computations presented here were performed by applying the central-difference algorithm with second- and fourth-order numerical dissipation according to Jameson. Time-accurate simulations were carried out by a dual time-stepping scheme that allows for convergence acceleration techniques such as multigrid and residual smoothing. The DES and the unsteady RANS, or URANS, simulations were run on three different hybrid grids, a URANS grid as well as a fine and a coarse DES grid, generated with GRIDGEN by Pointwise®. The left half of the entire aircraft, including the wing, the stabilizers, the fuselage, the cavity, and the telescope structure, is represented in the models. The URANS grid and the coarse and the fine DES grids consist of about 6×10^6, 14×10^6, and 20×10^6 total grid points, respectively. The boundary layers evolving on the viscous walls were resolved by prisms extruded from the triangulated surface mesh. Thirty-eight prism layers were placed on the surface of the fuselage and the wing, yielding a y^+ value of 1 at the node closest to the wall and a total prism stack height of 150% of the local boundary-layer thickness. The boundary layer evolving on the walls inside the cavity were covered with 28 prism layers. The rest of the computational domain was filled up with tetrahedra. In the DES mesh, the LES zone around the shear layer was discretized by a structured block of nearly isotropic hexahedra to resolve the small-scale turbulent structures of the shear layer. Figures 3a and 3b shows the DES grid in the vicinity of the cavity. Figure 3a shows a cut through the mesh in the plane perpendicular to the flight direction through the center of the primary mirror. Figure 3b shows a cut through the center plane of the cavity parallel to the line of sight of the telescope, which is elevated by 40 deg in reference to the horizon. In the URANS mesh, the shear layer was resolved by significantly coarser tetrahedral cells.

The physical time-step sizes and the durations of the simulation periods are listed in Table 1 for the conducted simulations. In the 7% wind-tunnel test, NASA used a scale factor of 0.061 to convert the frequency in wind-tunnel scale to the frequency in full scale at 41,000 ft of altitude.

Next, 180 and 40 inner iterations were performed per physical time step in the URANS and DES simulations, respectively. All simulations were carried out on 1020 processor cores in parallel on the HLRB2 supercomputer at the Leibniz Rechenzentrum in Garching, Germany. The simulation of 0.1 s wind-tunnel time took 48,000 CPUh with URANS and 180,000 CPUh with the DES (fine grid). For the considered configuration and a given time period, the total computational cost of the DES is higher by a factor of 3.8 than the cost for an equivalent URANS simulation.

B. Acoustic Simulation

Acoustic simulations were performed to predict the mode shapes and frequencies of the acoustic resonances inside the SOFIA telescope port. Assuming periodic time dependence $\exp(-i\omega t)$, where $\omega \in \mathbb{C}$ is the circular frequency, the wave equation can be reduced to the Helmholtz equation [8]:

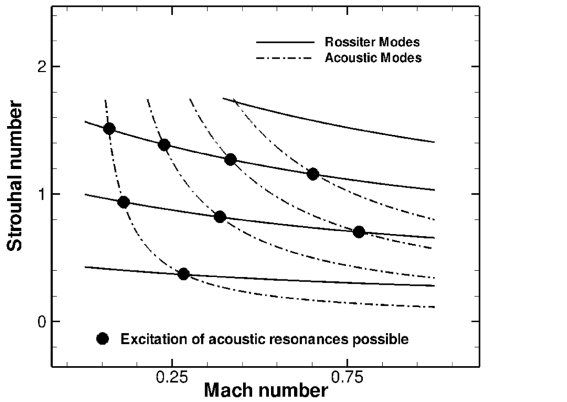

Fig. 2 Coincidence of Rossiter modes with acoustic resonance modes (rectangular 2-D cavity).

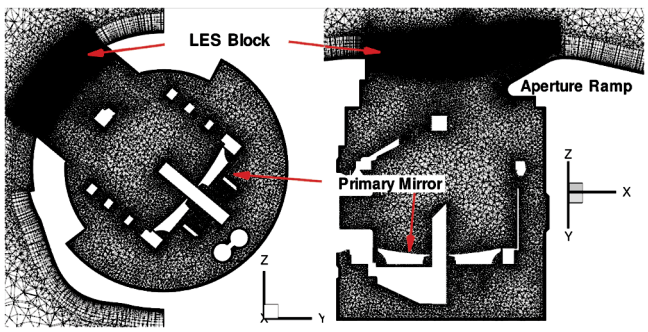

Fig. 3 Cuts through the DES grid: a) perpendicular to the flight direction, and b) parallel to the line of sight.

Table 1 Temporal resolution

Simulation	URANS		DES	
	Under wind-tunnel conditions	Scaled to flight conditions	Under wind-tunnel conditions	Scaled to flight conditions
Simulation period, s	0.33	5.4	0.05	0.82
Physical time-step size, μs	33	540	5	82

$$\left(\frac{\partial^2}{\partial x^2}+\frac{\partial^2}{\partial y^2}+\frac{\partial^2}{\partial z^2}\right)\phi(x,y,z)+K^2\phi(x,y,z)=0 \qquad (3)$$

for the velocity potential $\phi(x, y, z)$. x, y, and z are the nondimensional Cartesian coordinates in three dimensions; $K=\omega\cdot l_{\text{ref}}/c$ $(K\in\mathbb{C})$ denotes the dimensionless frequency, with $K/2\pi$ being the Helmholtz number. The time-dependent dimensionless disturbance velocity and pressure are given by $\mathbf{v}(x,y,z)=\nabla\phi$ and $p(x,y,z)=iK\phi$. Furthermore, l_{ref} and p are the characteristic reference length and the ambient pressure, respectively. The real part of the nondimensional frequency $\text{Re}\{K/2\pi\}$ corresponds to the resonant frequency, and the imaginary part $\text{Im}\{K/2\pi\}$ is a measure for the radiation loss. The quality factor $Q=|\text{Re}(K)/(2\text{Im}(K))|$ is the ratio of the time-averaged energy stored in the resonator to the energy loss per cycle, or, equivalently, the ratio of the center frequency to the bandwidth at the resonant frequency.

The main challenge of this approach is the specification of nonreflecting boundaries that satisfy the radiation condition. The infinite domain has to be truncated without causing unphysical reflections that may lead to large errors. In the present study, this has been performed with the perfectly matched layer (PML) approach according to Berenger [9], which is based on the complex scaling method. Within the finite PML zone, fictitious damping terms lead to an exponential decay of $\phi(x, y, z)$ as $|x|$, $|y|$, and $|z|$ go to infinity. A definite drawback of the present approach is the neglect of mean flow. However, it has been shown by Hu [10] that the mean flow can be included in a PML computation. As the Mach number is basically below 0.1 throughout the entire SOFIA cavity, the effect of the mean flow can be considered of minor impact in the present study.

The computational domain was discretized by finite elements, and a standard eigenvalue problem algorithm was used to solve the corresponding eigenvalue problem. The numerical grid that was used for the acoustic simulations represents the entire cavity, including the telescope structure and the vicinity of the fuselage close to the opening. It was also generated with the software GRIDGEN and consisted of 240,000 tetrahedra in total. The computations were carried out with the high-order finite element solver NGSOLVE by Joachim Schöberl [11].

IV. Results

A. Baseline Stratospheric Observatory for Infrared Astronomy Configuration

Figures 4a and 4b show the vorticity distributions in the shear layer as predicted by the URANS and DES. The URANS model yields a quite smooth and regular shear layer with a high level of coherence in the streamwise and transversal directions and a minor temporal variation as depicted in Fig. 4a. In contrast to the URANS, the DES reveals distinct three-dimensional features that are known to be the result of flow instability as it occurs in free shear layers, depicted in Fig. 4b. After a certain streamwise distance downstream of the cavity front edge, Kelvin–Helmholtz vortices evolve and grow as they are convected along the shear layer. The quite regular and quasi-two-dimensional vortices burst into chaotic and three-dimensional structures at a downstream position of about 50% of the cavity length. The number and size of the prevailing eddies are a hint of an energy cascading process. The Reynolds number in the experiments and in the computational fluid dynamics simulation was $13\times10^6/\text{m}$.

For the 7% wind-tunnel model by NASA in the 14×14 ft transonic wind-tunnel at the NASA Ames Research Center, the unsteady pressure history was measured at 56 different locations (see Fig. 5) on the telescope's surface [12]. The transformation to the frequency domain was carried out by discrete Fourier transform, applying the Welch method in combination with the Hanning window function [13]. Figures 6a–6d compare the pressure power spectral densities (PSDs) from the URANS and DES simulations with wind-tunnel measurements for two sensors, 9 and 41, on the primary mirror and the head-ring structure of the telescope assembly, as shown in Fig. 5. Amplitudes and frequencies have been scaled from wind-tunnel conditions to flight conditions.

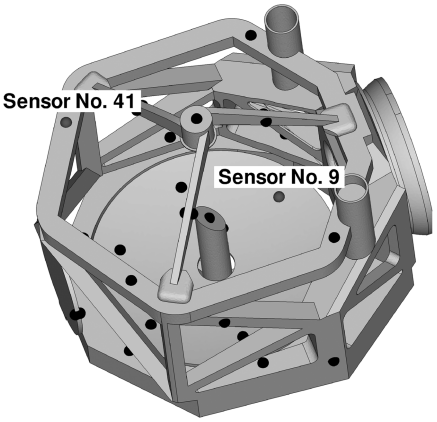

Fig. 5 Sensor positions.

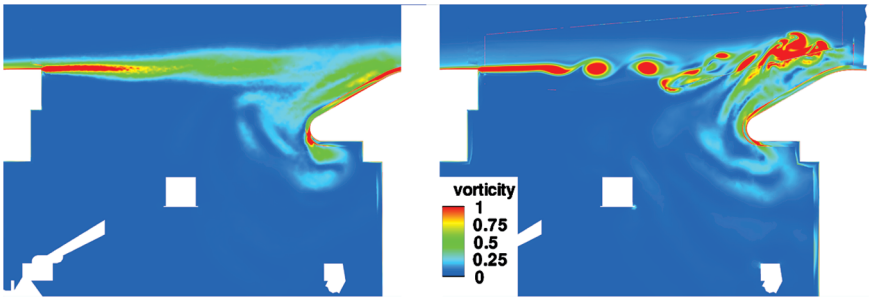

Fig. 4 Snaphots of the predicted vorticity in the shear layer region: a) URANS, and b) DES.

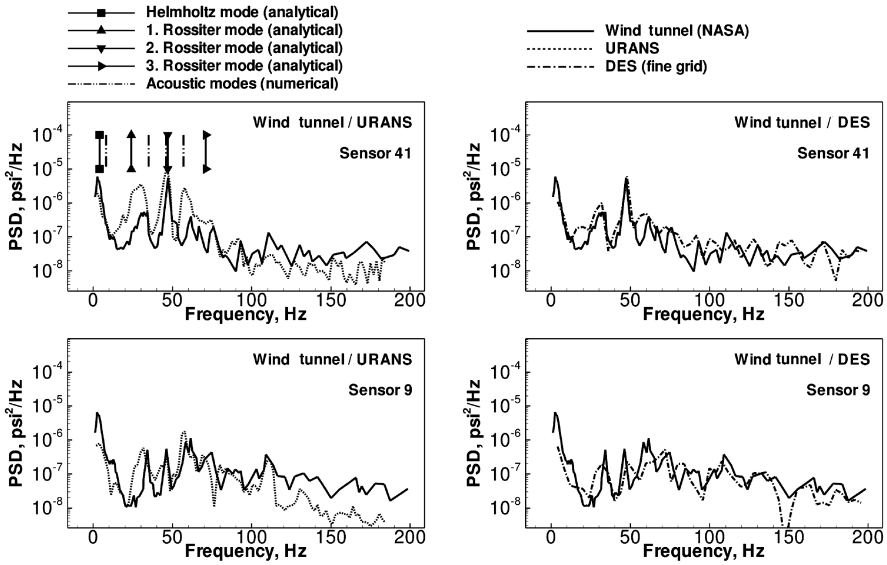

Fig. 6 Comparison of the pressure PSD predicted by the URANS and DES with wind-tunnel data. For sensor locations, refer to Fig. 5.

In the PSD plots, the peaks above 6 Hz are caused by acoustic resonance modes. Some of them are believed to be amplified and maintained by the Rossiter feedback process described earlier. Equation (1) yields 24, 47, and 71 Hz for the first, second, and third Rossiter modes, respectively, whereas the acoustic resonant frequencies of the cavity including the telescope have been computed to 8, 35, 47, and 60 Hz by solving the homogenous Helmholtz equation inside the open telescope port. The low-frequency peak at around 4 Hz is the footprint of a Helmholtz mode, which can be understood as an in-phase breathing of the cavity. The corresponding wavelength is larger by a factor of approximately 10 compared with the maximum dimension of the cavity. Its contribution to the image motion is low, as the pressure loads are nearly in phase over the entire telescope surface and thereby compensate each other. The frequencies of the analytically determined Helmholtz mode, the Rossiter modes, and the numerically predicted acoustic modes are indicated in Fig. 6a.

The frequencies of the characteristic peaks at around 35, 47, and 60 Hz are well predicted both by the URANS and DES, whereas the DES shows better agreement with the experiment. The URANS underpredicts amplitudes above 80 Hz; the DES shows an excellent agreement within the entire frequency range. The amplitudes predicted by the DES on the coarse grid (not shown here) were predicted too high, presumably because the turbulent structures of the shear layer were not resolved appropriately. The uncertainty of the URANS data with respect to amplitudes is likely to be attributed to shortcomings of the turbulence model.

Figures 7a–7c visualize some dominant acoustic modes of the baseline SOFIA telescope port as predicted by the homogenous Helmholtz equation. The contours represent the absolute values of the computed eigenvectors and can be interpreted as pressure fluctuations. The mode in Fig. 7a is the first organ pipe mode at around 8 Hz, the mode in Fig. 7c at around 60 Hz is three coupled standing waves in all three directions with a wavelength close to the cavity dimensions.

B. Passive Shear Layer Control

As pointed out earlier, the unsteady flowfield inside and around the cavity depends highly on the characteristics of the boundary layer upstream of the cavity. In general, thick boundary layers with high momentum loss show a more stable behavior of the free shear layer and yield lower sound-pressure levels inside the cavity. A further crucial factor is the three dimensionality of the shear layer. Shear layers with a very smooth shape and a high level of coherence in the lateral direction convect and amplify disturbances more efficiently than highly three-dimensional and incoherent shear layers.

Both of these effects can be capitalized to control unsteady cavity flow. Several numerical and experimental investigations have shown the efficiency of this approach using different concepts. Rossiter [1], Shaw [14], and Baysal et al. [15] demonstrated the positive impact of flat spoilers in front of the cavity. Barakos et al. [16] and Comte et al. [17] proved a sawtoothlike spoiler and a rod in crossflow to be

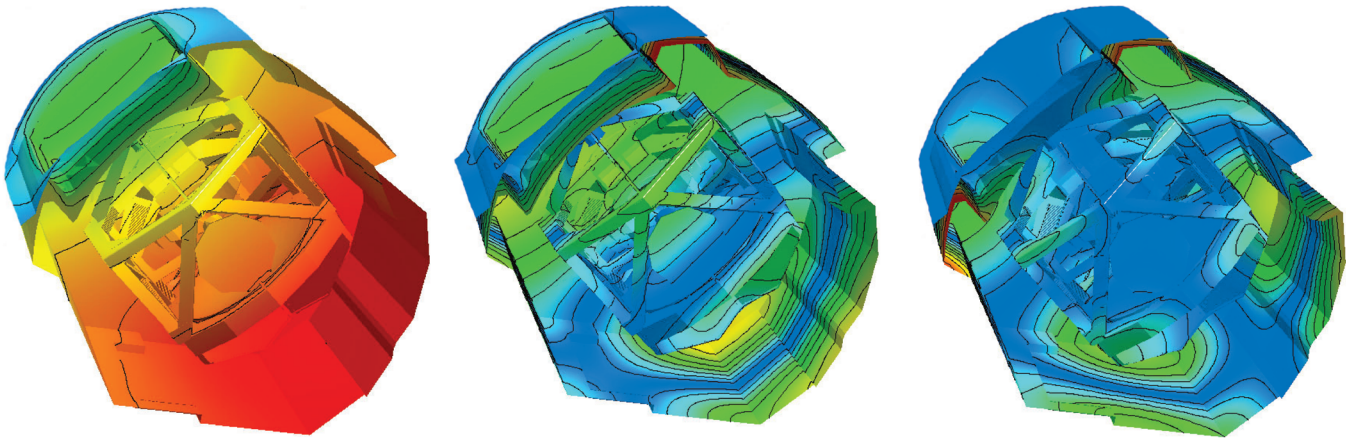

Fig. 7 Acoustic cavity modes predicted by solving the homogenous Helmholtz equation: a) first organ pipe mode at around 8 Hz, b) acoustic mode at 47 Hz, and c) acoustic mode with a wavelength close to the cavity dimensions in each direction at around 60 Hz. The contours represent the absolute values of the computed eigenvectors and can be interpreted as pressure fluctuations.

effective means for the suppression of unsteady pressure fluctuations. In the present study, the concept of Heller and Bliss [18] was investigated to mitigate the pressure fluctuations inside the SOFIA telescope port. Five pairs of vortex generators were installed in front of the cavity, each creating a pair of counter-rotating vortices in the streamwise direction.

Figure 8a shows a visualization of the shear layer above the telescope at three different streamwise positions right behind the vortex generators as predicted by URANS. The PSD plot in Fig. 8b reveals the impact of this concept on the fluctuation magnitude. The PSD is reduced within the frequency range of 10–90 Hz, which contributes most to the telescope's vibration. A slight increase of the Helmholtz mode around 4 Hz is observed due to the vortex generators. This phenomenon has already been encountered by Tramel et al. [19], who installed a porous fence upstream of the open cavity. Although the Helmholtz mode strengthened due to the presence of the fence, the overall sound-pressure level was decreased by 3–6 dB.

The reduction in the pressure fluctuations can be attributed to the aforementioned effects. The increase of shear layer thickness and the decrease of spatial coherence reduce the amplification of disturbances and their feedback. The drop in overall sound-pressure level on the surface of the telescope is predicted to be up to 10 dB locally due to the presence of the vortex generators. Nevertheless, it should be mentioned that the concept has two major drawbacks that have not been considered in the present investigation. The optical properties of the shear layer are affected adversely and the image quality in the optical and near infrared range is deteriorated. Furthermore the vortex generators increase the total drag of the aircraft.

C. Control of Cavity Resonant Frequencies

The magnitude of forced oscillations in general depends on both the frequency and the amplitude of the excitation source. When the excitation frequency approaches the natural frequency of the oscillator, the amount of transferred energy reaches its maximum. Some of the various structural resonance modes of the telescope assembly are close to the acoustic modes of the SOFIA cavity. A slight variation in acoustic resonance frequency may have a significant impact on the telescope's oscillations.

McIntyre predicted the influence of the variation in acoustic mode frequency on the performance of the telescope [20]. The end-to-end pointing simulation model he used in his analyses allowed for the computation of the telescope's pointing stability under realistic observing conditions. The simulation accounts for all disturbances acting on the system as well as the telescope's structural dynamics and the implemented controllers. Based on the disturbance input, the simulation model yields the root mean square of the angular image displacement in the telescope's focal plane. The angular deviation of the actual image position from the reference position is measured in arcseconds. By stretching the time axis of the pressure signals that were recorded in wind-tunnel experiments, McIntyre predicted the influence of slightly changed acoustic resonant frequencies (f_{sim}) on the telescope pointing stability [21]. According to the model he used in his analysis, frequency shifts within a range of $\pm 6\%$ significantly influenced the excitation of the telescope structure and the resulting image stability, as shown in Fig. 9.

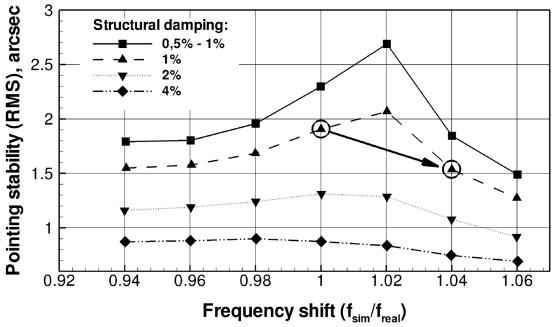

Fig. 9 Impact of frequency shift on telescope pointing stability, predicted by McIntyre [20].

Assuming a global structural damping of 1%, the pointing stability of the telescope deteriorates by 0.2 arcsec when the frequency is increased by 2%, but improves by almost 0.4 arcsec when the frequency is increased by 4%. An improvement can also be observed when the frequency of the aeroacoustic pressure fluctuations is reduced.

The approach of this study intends to estimate the possible range of shift in the acoustic resonant frequency of the SOFIA cavity to increase the gap between structural and acoustic resonance frequencies. According to Eq. (2), the characteristic resonant frequencies of an open cavity depend on the speed of sound and on the cavity's spatial dimensions. Decreasing L, D, or W leads to an increase of the acoustic resonant frequency. The speed of sound inside the cavity depends basically on the recovery temperature, which is a function of altitude and flight Mach number.

To assess the effect of geometrical changes, acoustic simulations of the SOFIA cavity have been performed for three different configurations, as shown in Fig. 10. The baseline cavity shape is shown in blue, the telescope structure in green, and the modified walls in orange. Configuration 2 (Fig. 10a) was basically reduced in diameter by installing additional walls. Configuration 2 (Fig. 10b) was shortened in length. And configuration 3 (Fig. 10c) contained acoustic baffles that decreased the spatial coherence of the cavity volume.

The impact of the cavity-wall modifications on the damping and frequency of the acoustic resonances is illustrated in Fig. 11 for the

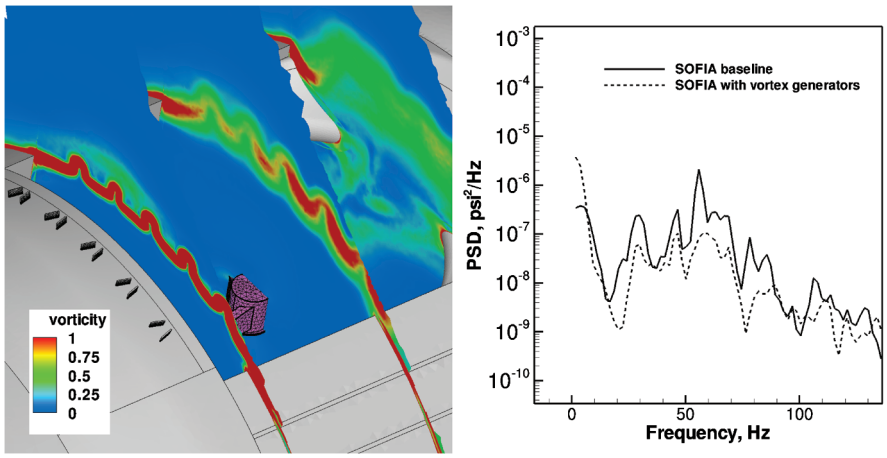

Fig. 8 Shown are the following: a) vortex generators placed upstream of the cavity, and b) impact of vortex generators on the PSD of sensor 9 as predicted by the URANS.

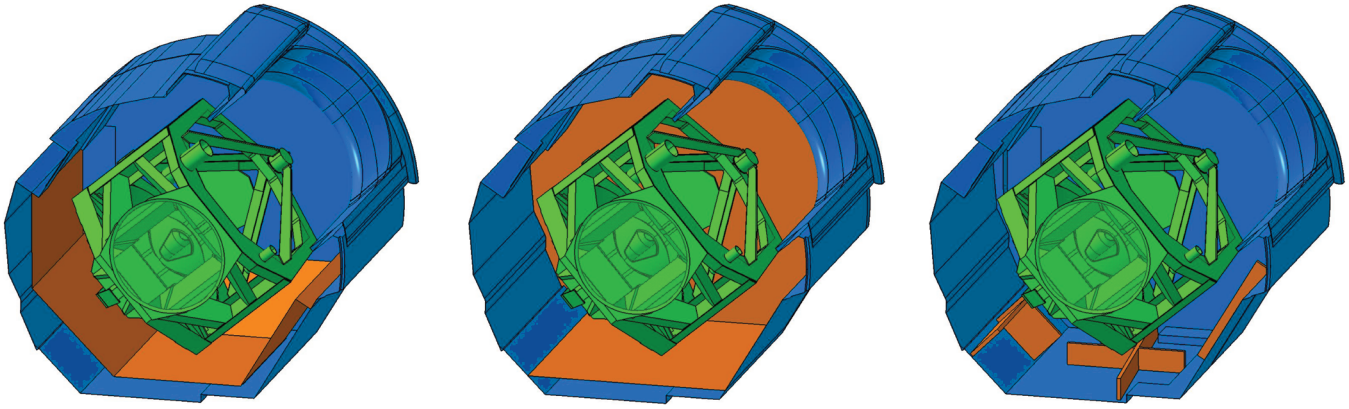

Fig. 10 Modified SOFIA telescope port geometries: a) configuration 2 with reduced cavity diameter, b) configuration 3 with partial reduced cavity diameter and reduced length, and c) configuration 3 with installed baffles.

modes at 8, 47, and 60 Hz. The shape of the acoustic mode at 8 Hz reveals this mode to be the first organ pipe mode of the cavity. Despite its distinct amplitude, there does not seem to be a dominant peak in the PSD, as it is overshadowed by the low-frequency Helmoltz mode around 4 Hz. The mode around 60 Hz is a highly symmetrical combination of standing acoustic waves in all three directions with wavelengths close to the cavity dimensions in the longitudinal and lateral directions.

The installed baffles show almost no effect on the low-frequency duct mode at 8 Hz. Neither the characteristic resonant frequency nor the damping properties change as the direction of the mode's fluid movement is basically oriented parallel to the baffle plates' surfaces. By contrast, the baffles have a significant influence on both the modes at higher frequencies, as the corresponding oscillations show components perpendicular to the baffles. The center frequency of the 47 and 60 Hz modes are reduced by 0.8 and 2 Hz, respectively. In contrast to the baffles, the reduction in the cavity dimensions yields an increase in resonant frequencies, as predicted by Eq. (2). This effect can be observed for all three modes and is most prominent for the 8 Hz mode of configuration 2; its frequency is shifted to a 10% higher value. Configuration 2 increases the center frequency of the 47 and 60 Hz modes by 1.5 and 7.0%, respectively, and configuration 3 shifts the frequencies by 2.8 and 3.6%, respectively.

The amount of acoustic energy radiated to the far field increases as the ratio of cavity volume to cavity opening surface decreases. This phenomenon, which can also be interpreted as an increasing acoustic damping, is observed in the simulation data for configurations 2 and 3. Except for the mode at 47 Hz, the absolute of the eigenvalues' imaginary part increases due to the reduction in the cavity volume.

The influence of flight Mach number on the recovery temperature inside the cavity was estimated assuming isotropic laws. The data measured in wind tunnel refer to an altitude of 41,000 ft and $M=$ 0.85. The change of recovery temperature due to the variation of the Mach number between $Ma = 0.8$ and 0.9 shifts the frequencies by $\pm 0.7\%$. Figure 12 shows the impact of both the cavity shape modifications and the flight Mach number variation on the resonant frequency (the shifted resonant frequency f is nondimensionalized by the characteristic resonant frequency f_0 of each mode).

The effects of flight Mach number variation and cavity shape modification combined, according to configuration 3, yield an

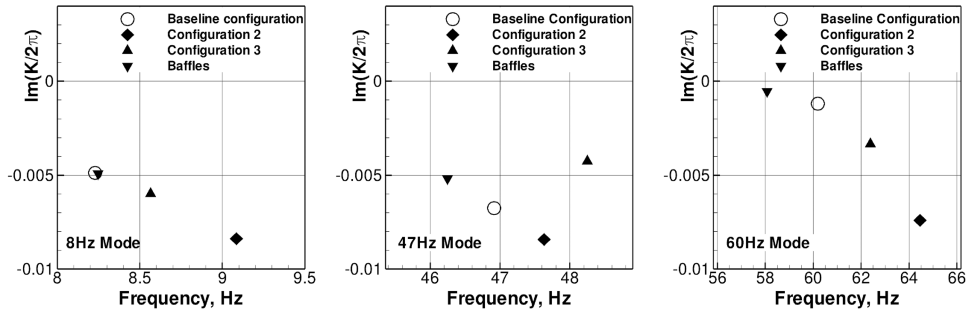

Fig. 11 Influence of cavity geometry on damping and frequency of acoustic resonance modes.

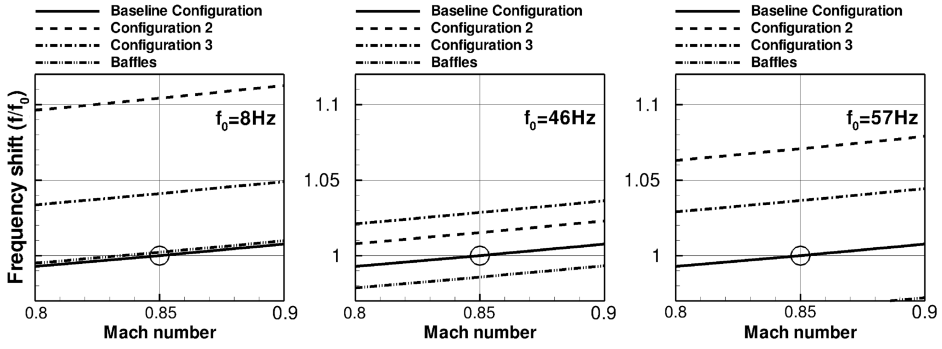

Fig. 12 Impact of cavity-wall modifications and flight Mach number on acoustic modes frequencies.

increase of 4.8, 3.6, and 4.4% for the three acoustic modes at 8, 47, and 60 Hz, respectively. In turn, by reducing the flight Mach number to a value of 0.8 and installing baffles, as depicted in Fig. 10c, the mode frequencies are decreased by −0.7, −2.1, and −4.2%. According to Fig. 9, the shift of the acoustic modes' frequency to both higher and lower values yields an improvement of the telescope's pointing stability.

V. Conclusions

The unsteady flow around the SOFIA was simulated by means of the URANS and DES; the acoustic resonance modes of the cavity have been computed by solving the homogenous Helmholtz equation. The comparison between the simulational and experimental data indicates that the prevailing flow physics and the acoustic phenomena are well predicted by the numerical model, the characteristic peaks of the PSD are captured both in amplitude and frequency, whereas the DES shows slightly better agreement in amplitudes.

The flow simulations show that pressure oscillations inside the cavity can be reduced significantly by modifying the stability characteristics of the shear layer. Vortex generators placed upstream of the SOFIA telescope port are revealed to be an effective means of passive flow control, by increasing the thickness of the shear layer and reducing the spatial coherence of the turbulent structures.

The frequencies of the acoustic modes could be shifted to lower and higher values by modifying the cavity shape or installing baffles inside the cavity. An increase of about 4% in resonance frequency could be achieved. According to the analyses by McIntyre, which are based on an end-to-end simulation model, this frequency shift yields an improvement of 0.4 arcsec in telescope pointing stability.

Acknowledgments

This project, grant 50OK0401, is being conducted on behalf of the DLR, German Aerospace Center and supported with funds from the Federal Ministry of Economics and Technology (BMWi), the state of Baden–Wuerttemberg, and the Universitaet Stuttgart. The author is responsible for the content.

References

[1] Rossiter, J. E., "Wind-Tunnel Experiments on the Flow over Rectangular Cavities at Subsonic and Transonic Speed," Aeronautical Research Council R&M No. 3438, London, UK, Oct. 1964.

[2] Rowley, C. W., "Modeling, Simulation, and Control of Cavity Flow Oscillations," Ph.D. Thesis, California Inst. of Technology, Pasadena, CA, Aug. 2001.

[3] Block, P. J. W., "Noise Response of Cavities of Varying Dimensions at Subsonic Speeds," NASA TN D-8351, Dec. 1976.

[4] Ahuja, K. K., and Mendoza, J., "Effects of Cavity Dimensions, Boundary Layer and Temperature on Cavity Noise with Emphasis on Benchmark Data to Validate Computational Aeroacoustic Codes," NASA CR-4653, April 1995.

[5] Gerhold, T., "Overview of the Hybrid RANS Code TAU," *Notes on Numerical Fluid Mechanics and Multidisciplinary Design*, edited by N. Kroll and J. K. Fassbender, Vol. 89, Springer, New York, 2005, pp. 81–92.

[6] Schmid, S., Lutz, T., and Krämer, E., "Numerical Simulation of the Flow Field Around the Stratospheric Observatory for Infrared Astronomy," *Notes on Numerical Fluid Mechanics and Multidisciplinary Design*, edited by C. Tropea, S. Jakirlic, H. J. Heinemann, R. Henke, and H. Hönlinger, Vol. 96, Springer, Berlin/Heidelberg/New York, 2007, pp. 364–371.

[7] Schmid, S., Lutz, T., and Krämer, E., "Simulation of the Unsteady Cavity Flow of the Stratospheric Observatory for Infrared Astronomy," *IUTAM Symposium on Unsteady Flows and Their Control*, Vol. 14, Springer, Berlin/Heidelberg/New York, 2009.

[8] Hein, S., Koch, W., and Schöberl, J., "Acoustic Resonances in a 2D High Lift Configuration and 3D Open Cavity," AIAA Paper 2005-2867, May 2005.

[9] Berenger, J.-P., "A Perfectly Matched Layer for the Absorption of Electromagnetic Waves," *Journal of Computational Physics*, Vol. 114, 1994, pp. 185–200. doi:10.1006/jcph.1994.1159

[10] Hu, F., "On Using Perfectly Matched Layer for the Euler Equations with a Non-Uniform Mean Flow," AIAA Paper 2004-2966, May 2004.

[11] Schöberl, J., "NETGEN An Advancing Front 2D/3D-Mesh Generator Based on Abstract Rules," *Computing and Visualization in Science*, Vol. 1, No. 1, 1997, pp. 41–52. doi:10.1007/s007910050004

[12] McIntyre, M., "Comparison of NASA and RSC Wind Tunnel Test Results," NASA Ames Research Center SOFIA TN MJM-012, April 2000.

[13] Oppenheim, A. V., and Schafer, R. W., "Smoothed Spectrum Estimators," *Digital Signal Processing*, Prentice–Hall, Englewood Cliffs, NJ, 1975, pp. 548–554.

[14] Shaw, L. L., "Suppression of Aerodynamically Induced Cavity Pressure Oscillations," *Journal of the Acoustical Society of America*, Vol. 66, No. 3, 1979, pp. 880–884. doi:10.1121/1.383242

[15] Baysal, O., Yen, G.-W., and Fouladi, K., "Navier–Stokes Computations of Cavity Aeroacoustics with Suppression Devices," *Journal of Vibration and Acoustics*, Vol. 116, No. 1, Jan. 1994, pp. 105–112. doi:10.1115/1.2930385

[16] Barakos, G. N., Lawson, S. J., Steijl, R., and Nayyar, P., "Assessment of Flow Control Devices for Transonic Cavity Flows using DES and LES," *IUTAM Symposium on Unsteady Separated Flows and Their Control*, Vol. 14, Springer, Berlin/Heidelberg/New York, 2009.

[17] Comte, P., Daude, F., and Mary, I., "Simulation of the Reduction of Unsteadiness in a Passively-Controlled Transonic Cavity Flow," *Journal of Fluids and Structures*, Vol. 24, No. 8, Nov. 2008, pp. 1252–1261. doi:10.1016/j.jfluidstructs.2008.08.001

[18] Heller, H. H., and Bliss, D. B., "The Physical Mechanism of Flow-Induced Pressure Fluctuations in Cavities and Concepts for Their Suppression," AIAA Paper 75-491, March 1975.

[19] Tramel, R., Rock, S., Ellis, J., and Sharpes, D., "Comparison of Large Cavity Aeroacoustic Computations with Flight Test Results," AIAA Paper 2005-2800, May 2005.

[20] McIntyre, M., "Sensitivity Study of Image Motion due to the Alignment of Cavity Aero-Acoustic Modes with TA Structural Modes," NASA Ames Research Center SOFIA TN MJM-009 Rev. 0, Aug. 1999.

[21] McIntyre, M., "SOFIA V Pressure Sensor Power Spectral Density Plots," NASA Ames Research Center SOFIA TN MJM-007 Rev. 0, July 1999.